Mitochondrial Communications 2 (2024) 38–47

Contents lists available at ScienceDirect

Mitochondrial Communications

journal homepage: www.keaipublishing.com/en/journals/mitochondrial-communications

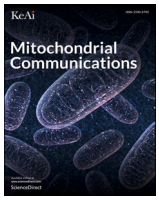

Research Article

Photobleaching and phototoxicity of mitochondria in live cell fluorescent super-resolution microscopy

Chia-Hung Lee [b], Douglas C. Wallace [c], Peter J. Burke [a,*]

[a] Department of Electrical Engineering and Computer Science, United States
[b] Department of Biomedical Engineering, University of California, Irvine, CA, 92697, United States
[c] Center for Mitochondrial and Epigenomic Medicine, Children's Hospital of Philadelphia and Department of Pediatrics, Division of Human Genetics, University of Pennsylvania, Philadelphia, PA, 19104, United States

ARTICLE INFO

Keywords:
Photobleaching
Phototoxicity
Mitochondria
Super-resolution
Fluorescent dye

ABSTRACT

Photobleaching and phototoxicity can induce detrimental effects on cell viability and compromise the integrity of collected data, particularly in studies utilizing super-resolution microscopes. Given the involvement of multiple factors, it is currently challenging to propose a single set of standards for assessing the potential of phototoxicity. The objective of this paper is to present empirical data on the effects of photobleaching and phototoxicity on mitochondria during super-resolution imaging of mitochondrial structure and function using Airyscan and the fluorescent structure dyes Mitotracker green (MTG), 10-N-nonyl acridine orange (NAO), and voltage dye Tetramethylrhodamine, Ethyl Ester (TMRE). We discern two related phenomena. First, phototoxicity causes a transformation of mitochondria from tubular to spherical shape, accompanied by a reduction in the number of cristae. Second, phototoxicity impacts the mitochondrial membrane potential. Through these parameters, we discovered that upon illumination, NAO is much more phototoxic to mitochondria compared to MTG or TMRE and that these parameters can be used to evaluate the relative phototoxicity of various mitochondrial dye-illumination combinations during mitochondrial imaging.

1. Introduction

Mitochondria are highly dynamic organelles, whose size, connectivity, and ultrastructure are controlled through balanced and dynamic cycles of fission, fusion, and cristae modifications. Analysis of mitochondrial structure and function is increasingly being recognized as central to understanding human health and disease.[1–6] Yet, mitochondria within tissue cells can have markedly different structures and functions.

In healthy cells, mitochondria form a tubular morphology (mitos being Greek for "thread"). Starting from the very first studies of the morphology of isolated mitochondria,[7,8] researchers have consistently observed that the morphology of the vital isolated mitochondria is spherical, either by using optical or electron microscopy. This includes our own work.[9,10] Since mitochondria fission/fusion has important physiological and clinical consequences,[11–13] the morphology of mitochondria under stress and toxic stimulus is an important topic in metabolism and cell biology, linked to a myriad of clinical pathologies.

Recent advances in live cell super-resolution microscopy have enabled imaging of mitochondrial ultrastructure.[14–29] However, the enhanced resolution achieved in super-resolution microscopes often comes at the expense of high-intensity illumination,[22] which can result in photobleaching and phototoxicity effects.[15,20,21,23,24,28,30–35] These effects have the potential to negatively impact cell viability and compromise the integrity of the collected data. A single set of standards for assessing the potential of phototoxicity cannot currently be proposed due to the involvement of multiple factors, such as illumination wavelength, intensity, duration, illumination regime, and sample characteristics.[23,32,36] Observing the degree of photobleaching is commonly used to evaluate photodamage,[37,38] but phototoxicity and photobleaching are distinct processes, with phototoxicity potentially occurring even before a noticeable decrease in imaging quality. More effective measures of mitochondrial phototoxicity could include reduced metabolic activity, compromised membrane integrity, DNA fragmentation, elevated reactive oxygen species (ROS), or initiation of apoptosis.[25,26,39,40] Efforts to reduce photobleaching and phototoxicity in super-resolution microscopy[27,28,41] include controlling light exposure,[29,37,38] using photostabilizing buffer,[42] or developing more stable fluorescent dyes.[19,24]

* Corresponding author.
E-mail address: pburke@uci.edu (P.J. Burke).

https://doi.org/10.1016/j.mitoco.2024.03.001
Received 2 October 2023; Received in revised form 21 February 2024; Accepted 11 March 2024
Available online 16 March 2024

Mitochondrial "sphericity" is one parameter of mitochondrial damage which has been associated with aging, apoptosis, and chemical insults.[43–49] Progressive sphericity has been observed using a variety of imaging systems including stimulated emission depletion (STED) microscopy and structured illumination microscopy (SIM), in association with photobleaching and phototoxicity (Supplement Table 4). Minamikawa et al.[31] found that Chloromethyl-X-rosamine (MitoTracker Red) was associated with potent phototoxicity at light doses of >2 J/cm^2 using confocal microscopy, in association with a rapid decrease of the mitochondrial membrane potential and a globular swelling of mitochondria. Wang et al.[24] developed a photostable fluorescent marker for STED microscopy, MitoPB Yellow, which had a high resistance to photobleaching and permitted monitoring of mitochondrial ultrastructural over an extended period of the mitochondria associated with experienced swelling and the loss of cristae, attributed to photodamage induced by the intense STED laser. Yang et al.[20] utilized the Hessian-SIM microscopy to show that extensive illumination induced rapid swelling of mitochondria, deformation and abruption of inner-membrane cristae, and round, hollow mitochondria. Liu et al.[19] developed a photostable fluorescent dye, PKMO, which drastically reduced the photobleaching and phototoxicity effects compared to other fluorescent dyes that lead to visible swelling and a drop in mitochondrial membrane potential. In summary, mitochondria, by empirical super-resolution microscopy data, tend to show loss of membrane potential and morphological changes from tubular to spherical as general responses to phototoxicity.

All of these new dyes as well as existing dyes such as but not limited to additional Mitotrackers (ThermoFisher) beyond the one we use here (Mitotracker Green, MTG), MitoBrilliant (Tocris), MitoView (Biotium), and PKMito (Spirochrome/cytoskeleton) point to the need for a solid understanding of the effects of photobleaching and phototoxicity on interpretation of imaging data. As many of the new dyes cited above are in the research and not commercially available yet, it is up to the authors of those research dye papers, as well as any future dye papers, to carefully use the techniques and methods we present in this paper on their own, or by seeding the dyes to other beta tester groups. This includes measuring the initial brightness, photobleaching rate, and phototoxicity. Such third-party evaluation would add considerable value to the entire mitochondrial community, which would further underline the importance of our methodology. Such a comprehensive study would be the ultimate goal of the initial work presented in this manuscript.

In order to begin this journey, we have decided to study the most broadly used, easiest-to-obtain dyes, that are compatible with all microscopes, from those in budget labs with only epi-fluorescence microscopy, to intermediate equipped confocal microscopy, to the well-funded labs with expensive advanced state of the art superresolution microscopes, such as STED, SIM, Airy, etc.[50,51] Therefore, this paper will have broad applicability to all mitochondria imaging studies.

The dyes MTG and NAO are the most commonly used structure dyes in the field of mitochondrial imaging. TMRE/TMRM is the most commonly used voltage dye, and in fact the only voltage dye in modern use. Many recent refs in the last 12 months show that these dyes continue to be the workhorse, mainstay, and defacto industry standard dyes in use to measure mitochondrial function and structure in standard and super-resolution microscopy.[52–58] While some data is available on the toxicity and bleaching of these dyes,[59,60] no comprehensive set of data has yet been presented. In this work, we present our carefully designed experimental data on the subject of the two related phenomena of photobleaching and phototoxicity. While the mechanisms of both of these are not well understood, our data provide a very important basis set on which to build models of mechanisms, and, practically, a guide for researchers in the field. In the end, we speculate on some mechanisms that may be responsible for the phenomena we observe.

Specifically, the fluorescent dye, NAO, is a widely used mitochondrial marker that binds to cardiolipin, a polyunsaturated acidic phospholipid localized in the mitochondrial inner membrane, providing clear images of cristae ultrastructure. However, NAO was reported to have cytotoxic effects when incubated at high concentrations[60] of an unknown mechanism. Victor et al.[61] proposed that NAO promotes strong membrane adhesion via van der Waals interactions between anti-parallel H-dimers of NAO molecules from the opposing bilayers, which led to the membrane remodeling of the mitochondria cristae. Using the Airyscan super-resolution microscope, we find that NAO exhibits a phototoxic effect causing rapid loss of fluorescence and membrane potential, which was separate from the cytotoxicity due to high concentration incubation. Employing TMRE as a voltage tracker and NAO or MTG as structure trackers, we found that both NAO and MTG could effectively act as fluorophores for imaging the mitochondrial membrane, but that NAO caused significant phototoxicity and loss of mitochondrial membrane potential.

2. Results

2.1. Photobleaching vs. phototoxicity

In an ideal world, the effects of photobleaching and phototoxicity would be unrelated, and could each be independently studied. Photobleaching could be studied via observation of the decay of fluorescence intensity vs. time. Phototoxicity, in this paper, is assayed via two metrics: 1) Change in mitochondrial morphology, from tubular to spherical, and 2) Change in mitochondria membrane potential, which would be (ideally) independently measured and observed.

A priori, several challenges exist already with such a research program/paradigm. First, and most obvious, phototoxicity and photobleaching may and typically do occur simultaneously. This complicates the interpretation and determination of cause/effect, if there is any relationship between the two. Second, with voltage dye TMRE (as well as other variations of fluorescence lipophilic cations such as rhodamine123 and JC1[62]), the loss of mitochondrial membrane potential causes loss of fluorescence intensity by definition of how it is employed with the Nernst equation. (For an up-to-date in-depth discussion of the voltage contrast mechanism, the reader is referred to our recent paper on the topic[63]). Therefore, a priori, one cannot distinguish between a voltage drop caused by phototoxicity leading to reduced fluorescence intensity and reduced fluorescence intensity caused by photobleaching. A third complication comes from the fact that virtually all dyes show some voltage-dependent binding, and are not purely structural labels. A more nuanced and subtle approach is necessary to decouple the two effects.

To address these complications, the are several possible avenues to explore. For TMRE one option is to study TMRE photobleaching independently, and then based on that data/experience, if TMRE intensity reduces faster than expected based on the photobleaching data, it must be due to reduced membrane potential. In fact, we find that to be the case in several of the experiments discussed below. Then, the voltage reduction due to phototoxicity can be independently determined from the photobleaching. Another option is to use morphology as the metric for phototoxicity, which can be measured even in the presence of photobleaching.

For the voltage dependence of structure dyes, one option is to quantify this. If the dye intensity changes more than the voltage dependence alone would predict, then it is due to photobleaching.

A postiori, we find that the use of two dyes NAO and TMRE at the same time causes phototoxicity (determined by morphology change and membrane potential drop) that is not caused by the individual dyes. This is explained in detail below.

2.2. NAO vs MTG photobleaching

In our first series of experiments, we set out to determine the relative photobleaching of structure dyes NAO vs MTG, independent of phototoxicity. Therefore we concentrate on the relative fluorescence intensity and ignore structural changes due to phototoxicity. Both dyes are known

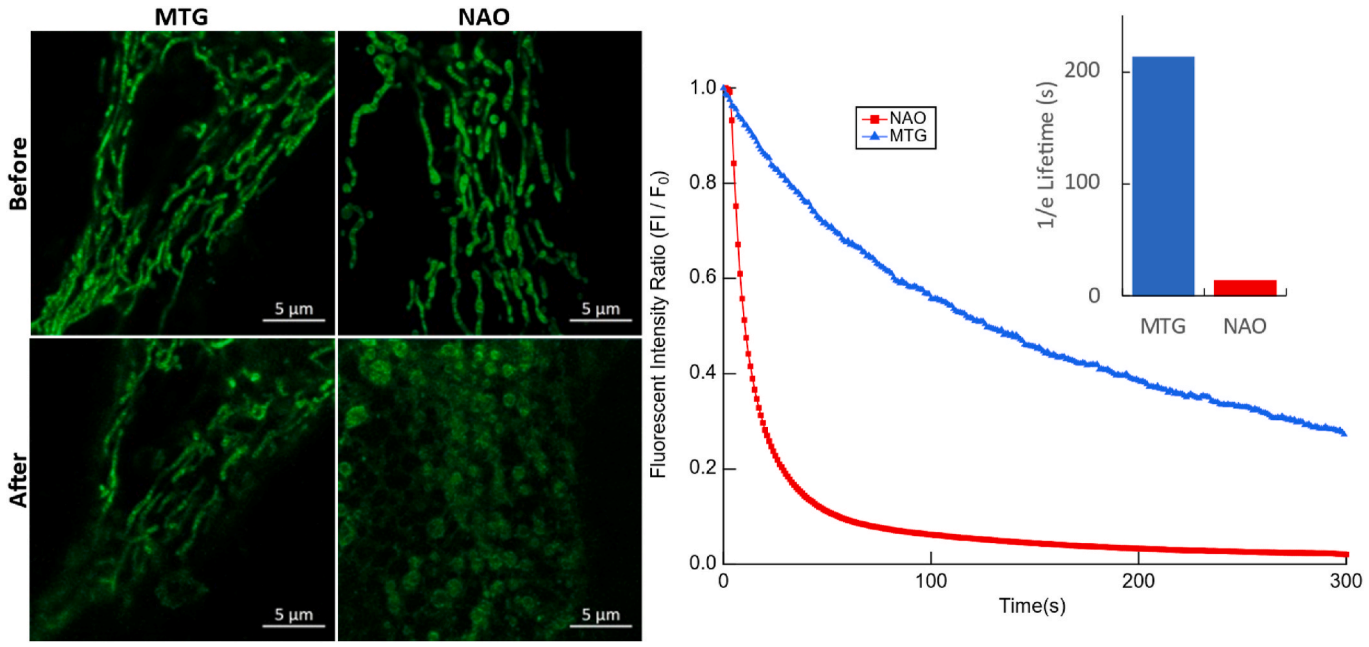

Fig. 1. Assessing photobleaching in time-lapse imaging with NAO and MTG. (A) Image of mitochondria stained with NAO and MTG before and after exposure to 488 nm illumination for 300 s. (B) NAO and MTG fluorescence intensities versus frames. N ≥ 3 independent experiments. (Intensity: 0.5 %; Pixel time: 3.54 μs; Time frame: 1 s).

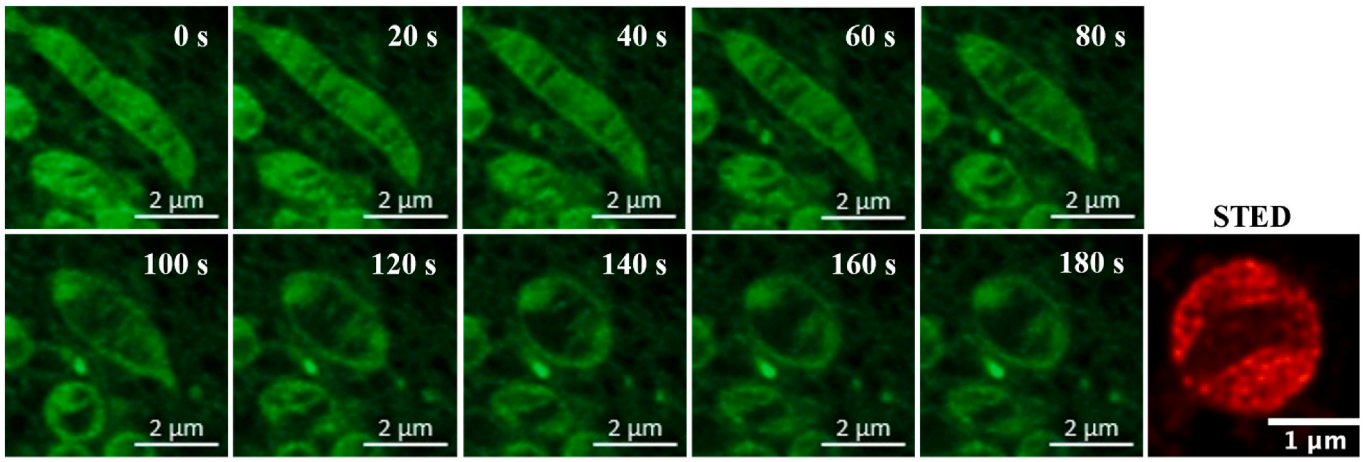

Fig. 2. Phototoxicity causes mitochondria ultrastructure to be destroyed. (Green) Time-lapse images of mitochondria stained with 100 nM NAO in HeLa cells using Zeiss Airyscan. (Red) Image with STED after sufficient time to cause mitochondria to become spherical shows similar morphology. N ≥ 3 independent experiments. (HeLa cell).

to localize in the mitochondria. NAO is known to have some dependence on mitochondrial membrane potential.[64–66] Quantitatively, it changes the fluorescence intensity of the organelle by about 50% upon complete depolarization of vital mitochondria. Therefore, any additional change in fluorescence intensity beyond this can be attributed to photobleaching.

The spectrum of NAO and MTG is similar (see Supplement 4 and 5), both being pumped at 488 nm with emission at around 520 nm. We observe that NAO manifests significantly faster photobleaching than MitoTracker Green (MTG). Fig. 1 shows a comparison of HeLa cells stained with MTG and NAO before and after 300 frames of exposure to 488 nm laser illumination. Note, all experiments in this manuscript are taken at a frame rate of 1 frame per second, and we use time in seconds in the x-axis to better present the changes in fluorescence and morphology over time. Each image had 572 pixels horizontal and vertical, with a dwell time of 3.54 μs per pixel, and the laser power set to 0.5 %. 100 % laser power is estimated at 1 mW.[67] In this test, the fluorescence intensity of mitochondria stained with MTG dye decreased by ~60 % during the experiment (The mean fluorescence intensity over all mitochondria within the entire cell) and the morphology of mitochondria retained the tubular structure before and after the illumination. On the other hand, the fluorescence intensity of mitochondria stained with NAO dye decreased by ~80 % in the first 50 frames and by ~90 % after 300 frames.

The loss of NAO intensity may be partially due to mitochondrial membrane potential change upon illumination (phototoxicity). However, the overall drop is over 90% (The mean fluorescence intensity dropped from 10312 AU to 213 AU). Therefore, at least part of the drop can be attributed to photobleaching. The photobleaching component of NAO is significantly faster than MTG. The 1/e lifetime value is 214 s for MTG and 14 s for NAO.

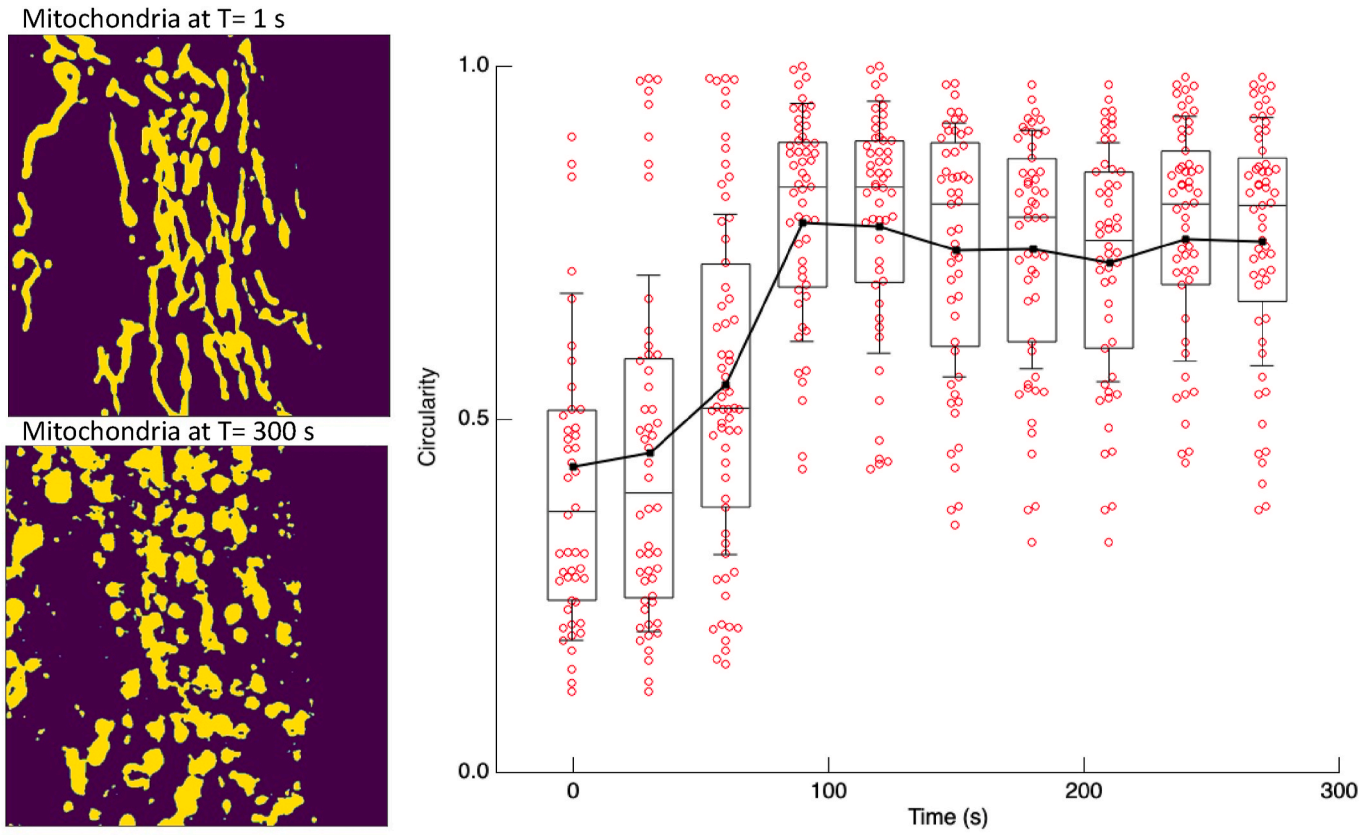

Fig. 3. Mitochondria segmentation and structure analysis. The binarization mask is used for single mitochondria analysis. The statistical analysis shows the change of circularity of mitochondria in cells through the time-lapse experiment. The mitochondria in the HeLa cell were stained with 100 nM NAO (Intensity: 0.5 %; Pixel time: 3.54 μs; Time frame: 1 s).

2.3. NAO vs MTG phototoxicity measured by morphology

Another phenomenon to access mitochondrial phototoxicity is the transformation of mitochondria from tubular to spherical shape. This is a non-reversible transformation different from mitochondria fission and fusion. Fig. 2 demonstrates time-lapse phototoxicity-induced ultrastructural changes of mitochondria in live cells, including changes to the outer morphology as well as the cristae structure. The mitochondria in HeLa cells were stained with 100 nM NAO and exposed to illumination with an excitation wavelength of 488 nm every 5 s for 60 frames. The filming time for each frame was 94 ms and we observed the mitochondria start to shrink into a spherical shape and the cristae

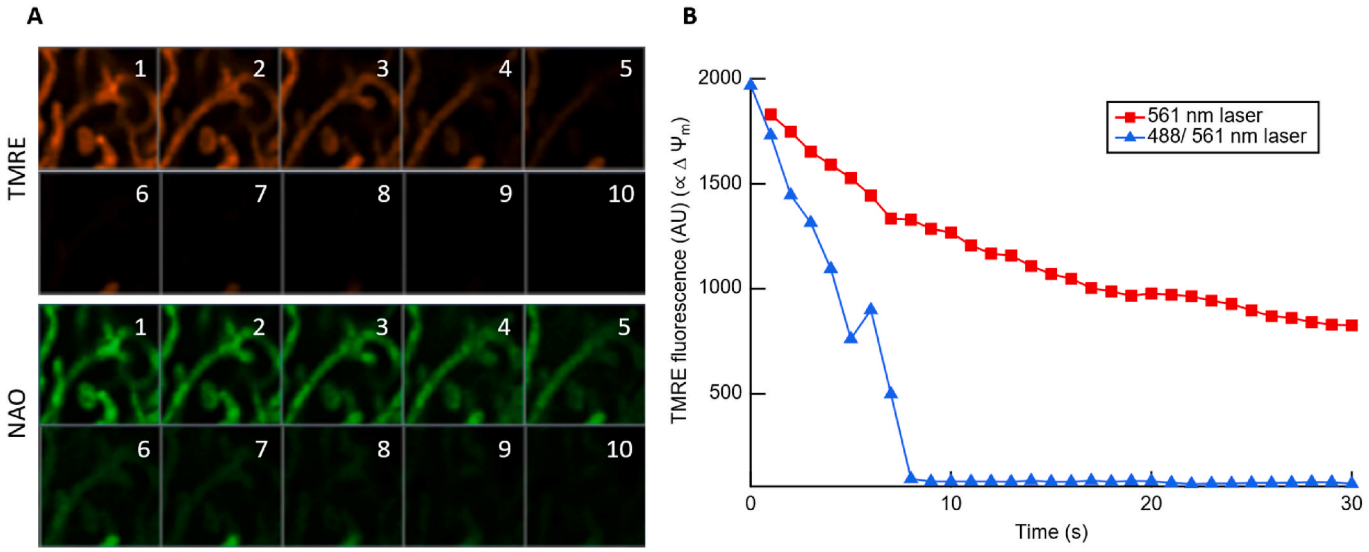

Fig. 4. Assessing NAO phototoxicity in loss of mitochondria membrane potential. (A) Time-lapse images of mitochondria in HeLa cells stained with 10 nM TMRE and 100 nM NAO, and exposure to 488 nm and 561 nm illuminations (Intensity: 0.5 %; Pixel time: 1.43 μs; Time frame: 1 s). (B) TMRE fluorescence intensity of mitochondria exposure to 561 nm only illuminations versus time.

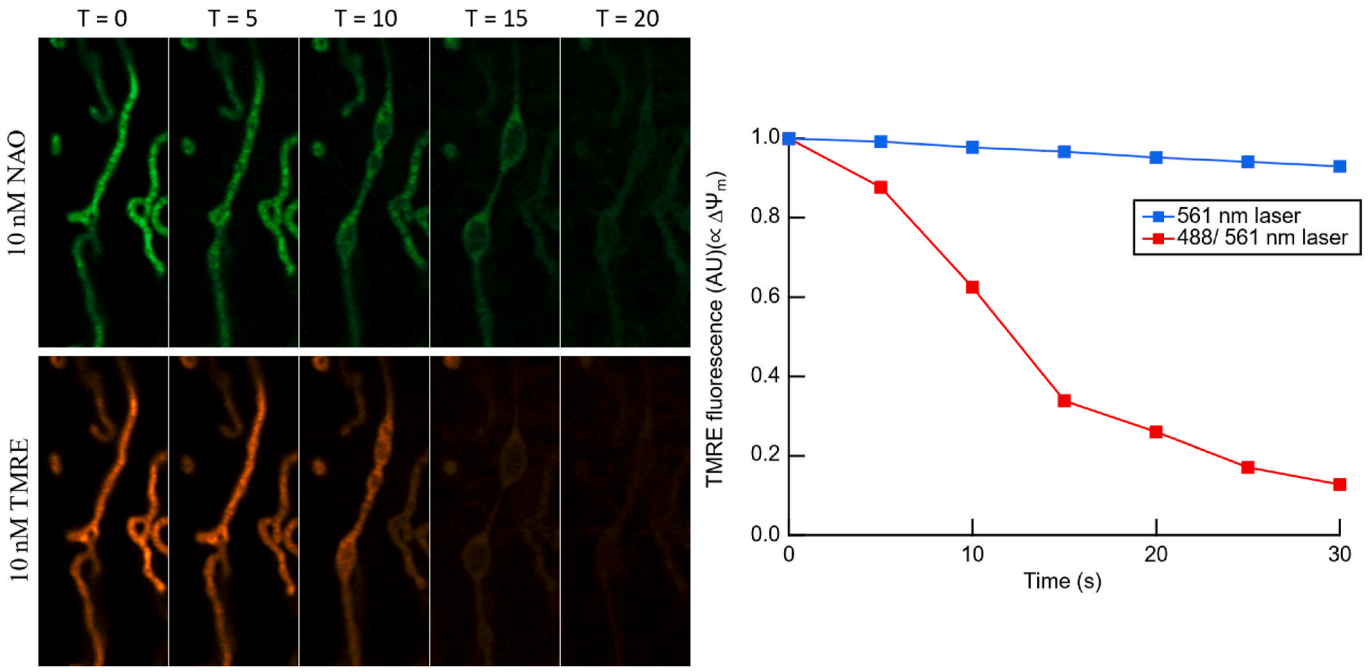

Fig. 5. Mitochondria stained with 10 nM NAO and 10 nM TMRE also experienced a rapid loss of fluorescence, loss of membrane potential, and morphological deformation when excited with 488/561 nm lasers. When excited with a 561 nm laser only, we did not observe the fast drop in TMRE intensity.

tended to stack toward two edges of the mitochondrion leaving a hollow space in the middle. The same result was also observed when imaging mitochondria in HeLa cells stained with 50 nM MTDR by using the stimulated emission depletion (STED) microscope.

Quantification of morphological changes was achieved following a detailed protocol that incorporated analysis software as described in Methods. This protocol assessed individual mitochondrial features in single cells (Supplement 1). To determine sphericity, we calculated the 2d circularity (as a stand-in for 3d sphericity) by the ratio of the perimeter to surface area. A perfectly spherical mitochondria will have a perimeter/area ratio of 2 pi r/(pi r^2). We define circularity as circularity $= 4\pi(\text{area}/\text{perimeter}^2)$, a circularity value of 1.0 indicates a perfect circle. As the value approaches 0.0, it indicates an increasingly elongated polygon (tubular). This dimensionless parameter was calculated using imaging processing software. An unsupervised K-means algorithm was used to determine the intensity threshold value of each image to accurately distinguish true mitochondria pixels from background fluorescence. Image thresholding and a binarization protocol allowed us to standardize and automate the selection of mitochondrial objects. The computer-identified mitochondria objects were manually inspected and compared to the original images before further morphology analysis using ImageJ.

During the timeframe of the above photobleach experiment (Fig. 1, 300 s), no morphology change was observed in the MTG case, indicating a lack of phototoxicity. In contrast, NAO illumination resulted in mitochondrial morphology changing from tubular to spherical, indicative of phototoxicity. NAO-stained mitochondria underwent a morphological change with the average circularity (a measure of phototoxicity) increasing from 0.4 to 0.7 within 100 s of illumination (Fig. 3). On the other hand, MTG-stained mitochondria maintained their tubular morphology through the illumination, with 0.2–0.4 for circularity (Supplement 6). This indicates NAO is significantly more phototoxic than MTG.

2.4. NAO vs MTG phototoxicity measured by membrane potential

In a second set of experiments, we aimed to assess phototoxicity through loss of membrane potential. We used TMRE to assess the membrane potential, a fluorescence dye that has a large dependence on membrane potential (changing over an order of magnitude on depolarization with FCCP, see e.g. Fig. 4c in Ref. 63).

We observed that prolonged exposure of NAO-stained mitochondria to 488 nm illumination reduced or even dissipated the mitochondrial membrane potential. Fig. 4A shows a time-lapse experiment of mitochondria stained with NAO and TMRE exposed to 488 nm and 561 nm illuminations. The 488 nm was used to excite NAO while 561 nm was used to excite TMRE. Both NAO and TMRE fluorescence disappeared after a couple of images were taken, which was different from our experience in multiple cell lines (HeLa, HEK293, and L6) stained with MTG and TMRE (Supplement 2). To further verify the cause of the membrane potential loss, we stained the mitochondria in live HeLa cells with NAO and TMRE dyes and exposed them to (a) 488 nm and 561 nm illuminations, and (b) only 561 nm illumination. Fig. 4B showed that for the group exposed to 488 nm and 561 nm illumination, both the NAO and TMRE fluorescence intensity dissipated over 90 % within the first 10 s. By contrast, when HeLa cells were interrogated with only the 561 nm illumination, the photobleaching effect was reduced, with TMRE fluorescence lasting for over 30 s before dropping to 50 %. Hence, we deduced that the rapid loss of NAO fluorescence and membrane potential can be attributed to the exposure of NAO to 488 nm illumination. This is a surprise and the mechanism is currently unknown.

The reduction in TMRE intensity alone when pumped at 561 nm may be due to either photobleaching or phototoxicity of TMRE. In this experiment alone, the two effects cannot be disentangled. This effect is also observed using other cell lines (Supplement 3). On the other hand, the rapid reduction in TMRE intensity upon an additional 488 nm illumination (used to pump the NAO) can be attributed to the phototoxicity of the NAO. This effect is not present when 488 and 561 nm are used simultaneously in the absence of NAO (Supplement 2).

2.5. Investigating the mechanism of NAO phototoxicity: comparison to high concentration experiments

A high concentration of NAO is known to trigger cytotoxicity even without excitation.[60] Under higher concentrations (>1 μM) than those used here, NAO inhibits cellular respiration and eventually triggers the

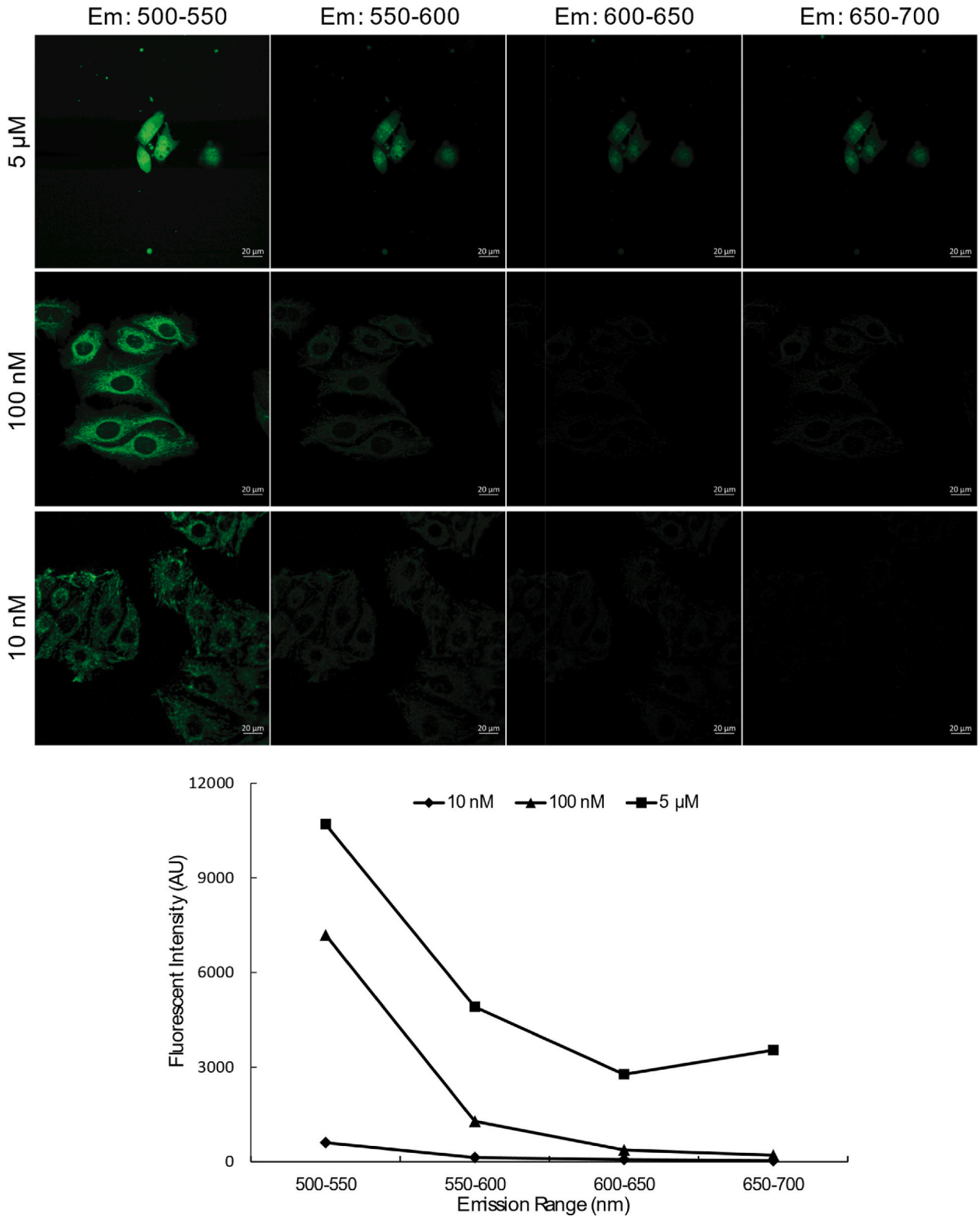

Fig. 6. 5 μM, 100 nM, and 10 nM NAO excited with 488 nm laser and measure emissions in 500–550 nm, 550–600 nm, 600–650 nm, 650–700 nm emission ranges.

morphological changes in mitochondria. Various mechanisms for this have been proposed. Victor et al.[61] proposed strong membrane-membrane adhesion would disrupt mitochondrial ultrastructure promoted by NAO under high concentration. This adhesion is proposed to be facilitated through van der Waals interactions between anti-parallel H-dimers of NAO molecules located in opposing bilayers. Consequently, this process is proposed to cause remodeling of the mitochondria cristae membranes. In their reported data, mouse embryonic fibroblasts (MEF) cells stained with high concentration (5 μM) of NAO demonstrated a shift in the emission range from λ_{em} = 525 nm–640 nm (green-to-red shift), as evidence of NAO H-dimer formation. On the other hand, cells stained with low concentration (5 nM) of NAO did not. In order to verify whether the observed rapid loss of fluorescence, loss of membrane potential, and morphological deformation that

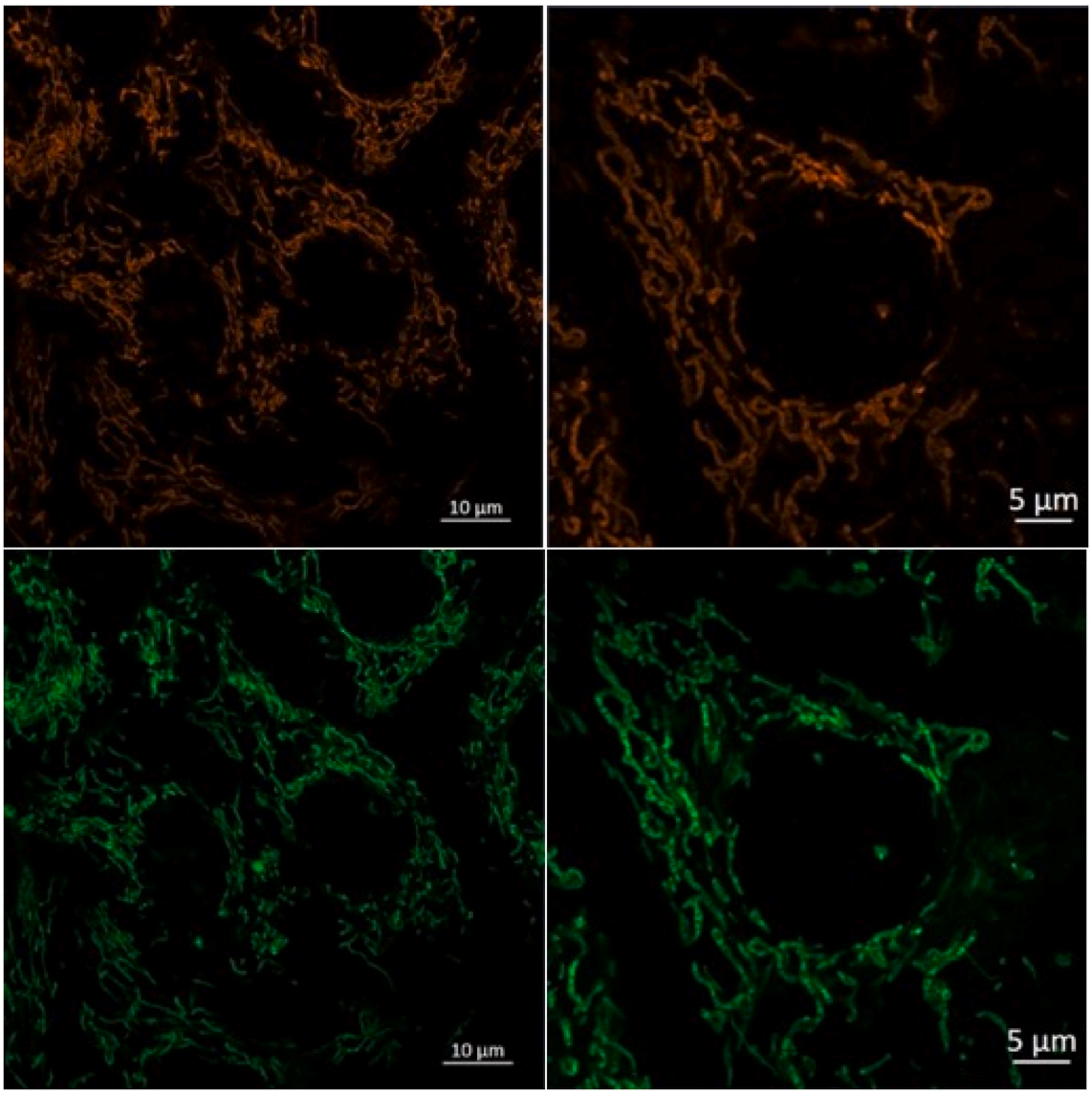

Fig. 7. Assessing cytotoxic effect through prolonged incubation time of NAO dyes in HEK293 cells. The HEK293 cells were stained with 100 nM NAO and 10 nM TMRE for 24 h before imaging. The mitochondria retained their tubular shapes and membrane potential. N = 3 independent experiments.

we observed above are the result of a high concentration cytotoxic effect observed by,[61] we repeated our above experiments with an even lower concentration of NAO (10 nM vs 100 nM) and found identical results, indicating that the phototoxicity we observed was not due to high concentration effects. Fig. 5 shows that even under 10 nM of NAO incubation, the mitochondria also experienced a rapid loss of fluorescence, loss of membrane potential, and morphological deformation. As above, these effects were also triggered by 488 nm laser excitation, which we did not observe when excited the mitochondria with 561 nm laser excitation only.

In order to confirm at our concentrations that NAO H-dimer was not occurring, we examined the occurrence of green-to-red emission shift. In Fig. 6, we used a 488 nm laser to excite mitochondria stained with NAO at concentrations of 10 nM, 100 nM, and 5 µM NAO. The emission ranges were set at 500–550 nm, 550–600 nm, 600–650 nm, and 650–700 nm. At concentrations of 10 nM and 100 nM, we observed the maximum emission in the expected 500–550 nm range, with unobservable emission in the 600–650 nm range associated with NAO H-dimers. However, at a concentration of 5 µM, a noticeable increase in emission intensity was observed in the 600–650 nm range. These results indicate that at the concentrations we used above, the dimerization-related mechanism is not responsible for the observed phototoxicity.

2.6. Investigating the mechanism of NAO phototoxicity: Verifying that toxicity is photo-induced

We also tested whether long-term incubation would trigger NAO cytotoxic effect at 100 nM concentration. We stained HEK293 cells with NAO and TMRE for 24 h instead of the normal 15 min. On subsequent imaging, we found that the mitochondria were intact and the membrane potential sustained (Fig. 7). Furthermore, once we excited the cells with a 488 nm laser, the rapid loss of fluorescence and the loss of mitochondrial membrane potential occurred. To further confirm that the phototoxicity of NAO required illumination, we used the laser scanning microscope to excite only a partial region of the cell and then imaged a wider region of the cell immediately. The red square in Fig. 8 was exposed to 488 nm illumination, and only the mitochondria inside the excited area demonstrated photobleaching, swelling, and membrane potential depolarization. Therefore, we conclude that 100 nM of NAO is lower than the concentration threshold to cause cytotoxic effects to mitochondria and the observed rapid loss of membrane potential and morphological deformation are phototoxic effects induced by NAO and

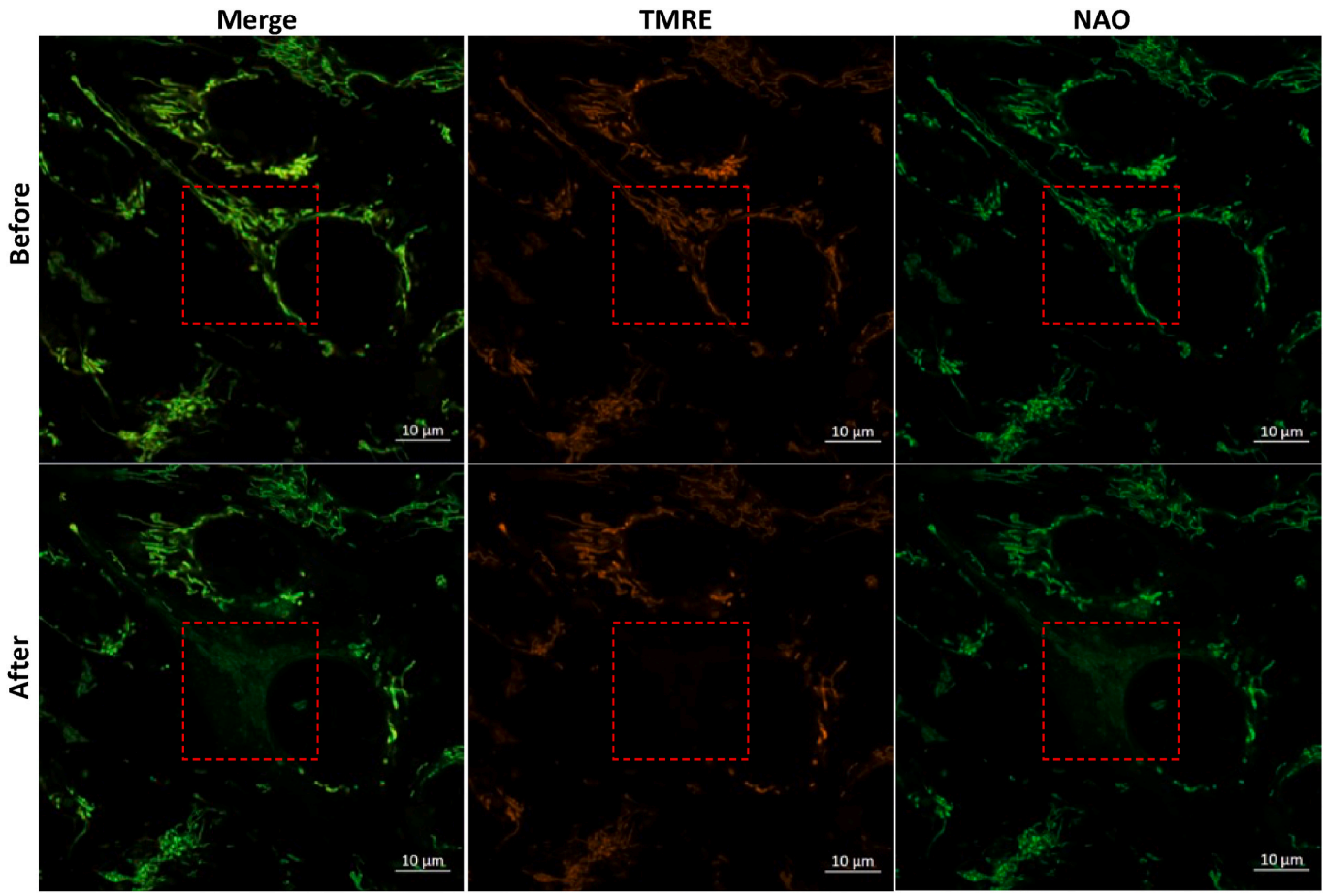

Fig. 8. Phototoxicity was restricted in the illuminated region of the cell. Live cell mitochondria stained with NAO only showed structural swelling and lost mitochondrial membrane potential in the region exposed to the 488 nm illumination. N ≥ 3 independent experiments.

488 nm laser excitation.

3. Conclusions

We have identified two useful parameters for evaluating the phototoxicity associated with the photobleaching of mitochondrially-targeted fluorescent dyes: conversion of tubular mitochondrial to spherical ones, and the loss of the mitochondrial membrane potential when the cell is co-stained with TMRE. Using these parameters, we have found that NAO-stained mitochondria illuminated at 488 nm undergo rapid loss of membrane potential and conversion from elongated to spherical mitochondria, while this is not the case when the cells are stained with MTG and illuminated at 488 nm. We also conclude that this effect is not related to concentration-induced cytotoxicity by NAO. It is currently unclear why NAO plus 488 nm illumination is so toxic but one possibility is that some derived product ruptures the mitochondrial inner membrane since TMRE fluorescence is lost with the same kinetics as the loss of the mitochondrial morphological integrity. In HeLa, HEK293, and L6 cells, NAO lost over 80 % of its fluorescence while MTG lost only 30% of its fluorescence in the first 50 s of illumination with the same settings. NAO-stained mitochondria underwent a morphological change with the average circularity (a measure of phototoxicity) increasing from 0.4 to 0.7 within 100 s of illumination. NAO-stained mitochondria lost their membrane potential rapidly after being exposed to 488 nm illumination (used to pump NAO), but this phenomenon was not observed when using 561 nm illumination (used to pump TMRE). Prolonged incubation with NAO demonstrated little or no toxicity to mitochondria, indicating that phototoxicity is the dominant toxicity mechanism of NAO.

4. Methods

4.1. Cell culture and fluorescent dye staining

The HEK293 cells and HeLa cells used in this research were purchased from ATCC. All the cells were cultured for 2−3 days in 75 cm^2 tissue flasks at 37 °C and 5 % CO_2 before being ready for experimentation. Dyes (10 nM TMRE and 100 nM MitoTracker Green (MTG) or 100 nM 10-N-nonyl acridine orange (NAO); Santa Cruz Biotechnology) were added to the cell culture media and incubated 1 h before the cell retrieval.

4.2. Live cell fluorescent microscopy of mitochondrial dynamics

The cells were seeded in CELLview 4-compartment glass-bottom tissue culture dishes (Greiner Bio-Ones, 627870), PS, 35/10 mm, 24 h before imaging. The live cell experiments were performed in the Zeiss LSM900 microscope with an incubation chamber (set to 37 °C). Imaging of cells was performed using Airyscan an alpha Plan-Apochromat 63 × /1.4 Oil DIC M27 objective. The laser powers were adjusted between approximately 0.3%–2%, and the master gain was between 750 and 900. We started continuous scanning at maximum speed at a zoom factor of 1, in order to obtain a relatively strong signal-to-noise ratio for imaging. Later, we brought the field of mitochondria of interest into view and stopped scanning. The pixel dwell time was set between 0.85 and 1.04 μs, respectively to avoid overtime exposure of mitochondria to the laser. NAO and MTG were used for structural imaging (labeling the lipid bilayer), and TMRE was used for voltage imaging, as explained in the main text.

4.3. Fluorescence intensity calculation in timelapse images

The calculation of fluorescence intensity in timelapse images (Fig. 1, Fig 4, and Fig. 5) is based on the following pipelines. An auto-threshold procedure (Otsu method) is first applied to segment out the object (mitochondria) from the background. Later, we averaged the whole values of the mitochondria pixels to get the average fluorescence intensity at each time point.

4.4. Image processing and mitochondrial quantification

Image processing and quantification were completed using Zeiss Zen 3.5 software, ImageJ, Igor Pro, OpenCV, and Python. Images were deconvoluted using the Airyscan Super-resolution processing function with the optimal auto-filter setting. Following deconvolution, a Gaussian blur filter was used to denoise the image, and a top hat morphological transformation was performed to subtract non-mitochondria objects using ImageJ. Using Python and OpenCV, we performed K-Means clustering to separate the image into 2 groups based on fluorescence intensity: mitochondria and non-mitochondria. In the time-lapse experiments, the photobleaching effect will result in worse recognition of mitochondria due to the dim fluorescence. Therefore, the mitochondria objects were manually inspected and compared to the original images before further morphology analysis using ImageJ. Finally, a particle analysis was done on the mitochondria group to measure the perimeter and circularity of mitochondria using ImageJ. Statistical analysis and plots were generated using Igor Pro. The ImageJ macro can be found in.[68]

CRediT authorship contribution statement

Chia-Hung Lee: Conceptualization, Data curation, Formal analysis, Methodology. **Douglas C. Wallace:** Supervision, Writing – review & editing. **Peter J. Burke:** Conceptualization, Funding acquisition, Project administration, Supervision, Writing – original draft, Writing – review & editing.

Declaration of competing interest

Dr. Douglas Wallace is the Honorary Editor for Mitochondrial Communications and was not involved in the editorial review or the decision to publish this article. Some of the authors are in the process of founding a company related to microfluidic mitochondrial assays.

Acknowledgments

We thank Kristofer Fertig and Dr. Christian Wurm for feedback and the loan of a demonstration STED system (ABBERIOR STEDYCON). This work was supported in part by NIH grant 1 R01 CA259635-01A1 and 3 R01 CA243033- 03S1A1, National Science Foundation (NSF) award #2153425, and Army Research Office through the ARO- (Contract Nos. W911NF-18-1-0076, W911NF2010103, and W911NF1910369) and the AFOSR (grant FA9550-23-1-0061). This material is based upon work supported by the Air Force Office of Scientific Research under award numbers FA9550-23-1-0436 and FA9550-23-1-0061. Any opinions, findings, and conclusions or recommendations expressed in this material are those of the author(s) and do not necessarily reflect the views of the United States Air Force.

Appendix A. Supplementary data

Supplementary data to this article can be found online at https://doi.org/10.1016/j.mitoco.2024.03.001.

References

1. Wallace DC, Fan W. Energetics, epigenetics, mitochondrial genetics. *Mitochondrion*. 2010;10:12–31.
2. Wallace DC. Mitochondrial DNA mutations in disease and aging. *Environ Mol Mutagen*. 2010;51:440–450.
3. Wallace DC. Bioenergetics, the origins of complexity, and the ascent of man. *Proc Natl Acad Sci USA*. 2010;107:8947–8953.
4. Wallace DC. Mitochondria and cancer. *Nat Rev Cancer*. 2012;12:685–698.
5. Wallace DC. Mitochondrial diseases in man and mouse. *Science*. 1999;283:1482–1488.
6. Wallace DC. Bioenergetic origins of complexity and disease. *Cold Spring Harbor Symp Quant Biol*. 2011;76:1–16.
7. Hackenbrock CR. Ultrastructural bases for metabolically linked mechanical activity in mitochondria. I. Reversible ultrastructural changes with change in metabolic steady state in isolated liver mitochondria. *J Cell Biol*. 1966;30:269–297.
8. Hackenbrock CR. Ultrastructural bases for metabolically linked mechanical activity in mitochondria. II. Electron transport-linked ultrastructural transformations in mitochondria. *J Cell Biol*. 1968;37:345–369.
9. Zand K, Pham T, Davila A, Wallace DC, Burke PJ. Nanofluidic platform for single mitochondria analysis using fluorescence microscopy. *Anal Chem*. 2013;85:6018–6025.
10. Zand K, et al. Resistive flow sensing of vital mitochondria with nanoelectrodes. *Mitochondrion*. 2017;37:8–16.
11. Chen H, Chan DC. Mitochondrial dynamics-fusion, fission, movement, and mitophagy-in neurodegenerative diseases. *Hum Mol Genet*. 2009;18:R169–R176.
12. Friedman JR, Nunnari J. Mitochondrial form and function. *Nature*. 2014;505:335–343.
13. Chan DC. Fusion and fission: interlinked processes critical for mitochondrial health. *Annu Rev Genet*. 2012;46:265–287.
14. Stephan T, Roesch A, Riedel D, Jakobs S. Live-cell STED nanoscopy of mitochondrial cristae. *Sci Rep*. 2019;9, 12419.
15. Yang X, et al. Mitochondrial dynamics quantitatively revealed by STED nanoscopy with an enhanced squaraine variant probe. *Nat Commun*. 2020;11:3699.
16. Huang X, et al. Fast, long-term, super-resolution imaging with Hessian structured illumination microscopy. *Nat Biotechnol*. 2018;36:451–459.
17. Guo Y, et al. Visualizing intracellular organelle and cytoskeletal interactions at nanoscale resolution on millisecond timescales. *Cell*. 2018;175:1430–1442.e17.
18. Kondadi AK, et al. Cristae undergo continuous cycles of membrane remodelling in a MICOS -dependent manner. *EMBO Rep*. 2020;21:1–22.
19. Liu T, et al. Multi-color live-cell STED nanoscopy of mitochondria with a gentle inner membrane stain. *Proc Natl Acad Sci U S A*. 2022;119.
20. Yang Z, et al. Cyclooctatetraene-conjugated cyanine mitochondrial probes minimize phototoxicity in fluorescence and nanoscopic imaging. *Chem Sci*. 2020;11:8506–8516.
21. Kilian N, et al. Assessing photodamage in live-cell STED microscopy. *Nat Methods*. 2018;15:755–756.
22. Waldchen S, Lehmann J, Klein T, Van De Linde S, Sauer M. Light-induced cell damage in live-cell super-resolution microscopy. *Sci Rep*. 2015;5:1–12.
23. Laissue PP, Alghamdi RA, Tomancak P, Reynaud EG, Shroff H. Assessing phototoxicity in live fluorescence imaging. *Nat Methods*. 2017;14:657–661.
24. Wang C, et al. A photostable fluorescent marker for the superresolution live imaging of the dynamic structure of the mitochondrial cristae. *Proc Natl Acad Sci USA*. 2019;116:15817–15822.
25. Ge J, et al. Standard fluorescent imaging of live cells is highly genotoxic. *Cytometry*. 2013;83 A:552–560.
26. Mutoh H, Perron A, Akemann W, Iwamoto Y, Knöpfel T. Optogenetic monitoring of membrane potentials. *Exp Physiol*. 2011;96:13–18.
27. Kwon J, Elgawish MS, Shim S-H. Bleaching-resistant super-resolution fluorescence microscopy. *Adv Sci*. 2022;9, e2101817.
28. Song Y, et al. Improving brightness and stability of Si-rhodamine for super-resolution imaging of mitochondria in living cells. *Anal Chem*. 2020;92:12137–12144.
29. Wolf DM, Segawa M, Shirihai OS, Liesa M. Method for live-cell super-resolution imaging of mitochondrial cristae and quantification of submitochondrial membrane potentials. *Methods Cell Biol*. 2020;155:545–555.
30. Ojha A, Ojha NK. Excitation light-induced phototoxicity during fluorescence imaging. *J Biosci*. 2021;46.
31. Minamikawa T, et al. Chloromethyl-X-rosamine (MitoTracker Red) photosensitises mitochondria and induces apoptosis in intact human cells. *J Cell Sci*. 1999;112:2419–2430.
32. Icha J, Weber M, Waters JC, Norden C. Phototoxicity in live fluorescence microscopy, and how to avoid it. *Bioessays*. 2017;39.
33. Wolf DM, et al. Individual cristae within the same mitochondrion display different membrane potentials and are functionally independent. *EMBO J*. 2019;38, e101056.
34. Jakobs S, Stephan T, Ilgen P, Brüser C. Light microscopy of mitochondria at the nanoscale. *Annu Rev Biophys*. 2020;49:289–308.
35. Chen Y, et al. Multi-color live-cell super-resolution volume imaging with multi-angle interference microscopy. *Nat Commun*. 2018;9.
36. Magidson V, Khodjakov A. Circumventing photodamage in live-cell microscopy. In: *Methods in Cell Biology*. vol. 114. Academic Press Inc.; 2013:545–560.
37. Mubaid F, Brown CM. Less is more: longer exposure times with low light intensity is less photo-toxic. *Micros Today*. 2017;25:26–35.
38. Boudreau C, et al. Excitation light dose engineering to reduce photo-bleaching and photo-toxicity. *Sci Rep*. 2016;6.

39. Markova L, Novohradsky V, Kasparkova J, Ruiz J, Brabec V. Dipyridophenazine iridium(III) complex as a phototoxic cancer stem cell selective, mitochondria targeting agent. *Chem Biol Interact*. 2022;360.
40. Ray RS, et al. Singlet oxygen mediated DNA damage induced phototoxicity by ketoprofen resulting in mitochondrial depolarization and lysosomal destabilization. *Toxicology*. 2013;314:229–237.
41. Tosheva KL, Yuan Y, Matos Pereira P, Culley S, Henriques R. Between life and death: strategies to reduce phototoxicity in super-resolution microscopy. *J Phys D Appl Phys*. 2020;53, 163001.
42. Stockley JH, et al. Surpassing light-induced cell damage in vitro with novel cell culture media. *Sci Rep*. 2017;7.
43. Klein Geltink RI, et al. Mitochondrial priming by CD28. *Cell*. 2017;171:385–397.e11.
44. Hibshman JD, Sherwood DR. *Acute and Intergenerational Nutrient Responses in Caenorhabditis elegans*. 2017.
45. Rasmussen ML, et al. MCL-1 inhibition by selective BH3 mimetics disrupts mitochondrial dynamics causing loss of viability and functionality of human cardiomyocytes. *iScience*. 2020;23, 101015.
46. Bahat A, et al. MTCH2-mediated mitochondrial fusion drives exit from naïve pluripotency in embryonic stem cells. *Nat Commun*. 2018;9:5132.
47. Bagamery LE, Justman QA, Garner EC, Murray AW. A putative bet-hedging strategy buffers budding yeast against environmental instability. *Curr Biol*. 2020;30:4563–4578.e4.
48. Cackovic J, et al. Vulnerable parkin loss-of-function Drosophila dopaminergic neurons have advanced mitochondrial aging, mitochondrial network loss and transiently reduced autophagosome recruitment. *Front Cell Neurosci*. 2018;12:1–14.
49. Balboa E, et al. MLN64 induces mitochondrial dysfunction associated with increased mitochondrial cholesterol content. *Redox Biol*. 2017;12:274–284.
50. Schermelleh L, et al. Super-resolution microscopy demystified. *Nat Cell Biol*. 2019;21:72–84.
51. Jacquemet G, Carisey AF, Hamidi H, Henriques R, Leterrier C. The cell biologist's guide to super-resolution microscopy. *J Cell Sci*. 2020;133.
52. Fry MY, et al. In situ architecture of Opa1-dependent mitochondrial cristae remodeling. *bioRxiv*. 2023. https://doi.org/10.1101/2023.01.16.524176.
53. Torrens-Mas M, et al. Mitochondrial functionality is regulated by alkylphospholipids in human colon cancer cells. *Biology*. 2023;12:1457.
54. Sagar S, et al. Obesity impairs cardiolipin-dependent mitophagy and therapeutic intercellular mitochondrial transfer ability of mesenchymal stem cells. *Cell Death Dis*. 2023;14:324.
55. Dong J, et al. Mic19 depletion impairs endoplasmic reticulum-mitochondrial contacts and mitochondrial lipid metabolism and triggers liver disease. *Nat Commun*. 2024;15:168.
56. Cinat D, et al. Mitophagy induction improves salivary gland stem/progenitor cell function by reducing senescence after irradiation. *Radiother Oncol*. 2024;190, 110028.
57. Zhang Z, et al. CGI1746 targets σ1R to modulate ferroptosis through mitochondria-associated membranes. *Nat Chem Biol*. 2024. https://doi.org/10.1038/s41589-023-01512-1.
58. Kok CY, et al. Ghrelin mediated cardioprotection using in vitro models of oxidative stress. *Gene Ther*. 2024. https://doi.org/10.1038/s41434-023-00435-9.
59. Scaduto RC, Grotyohann LW. Measurement of mitochondrial membrane potential using fluorescent rhodamine derivatives. *Biophys J*. 1999;76:469–477.
60. Septinus M, Berthold Th, Naujok A, Zimmermann HW. [Hydrophobic acridine dyes for fluorescent staining of mitochondria in living cells. 3. Specific accumulation of the fluorescent dye NAO on the mitochondrial membranes in HeLa cells by hydrophobic interaction. Depression of respiratory activity, changes in the ultrastructure of mitochondria due to NAO. Increase of fluorescence in vital stained mitochondria in situ by irradiation]. *Histochemistry*. 1985;82:51–66.
61. Almendro-Vedia VG, et al. Supramolecular zippers elicit interbilayer adhesion of membranes producing cell death. *Biochim Biophys Acta Gen Subj*. 2018;1862:2824–2834.
62. Vianello C, et al. High-throughput microscopy analysis of mitochondrial membrane potential in 2D and 3D models. *Cells*. 2023;12:1089.
63. Lee C, Wallace DC, Burke PJ. Super-resolution imaging of voltages in the interior of individual, vital mitochondria. *ACS Nano*. 2024;18:1345–1356.
64. Jacobson J, Duchen MR, Heales SJR. Intracellular distribution of the fluorescent dye nonyl acridine orange responds to the mitochondrial membrane potential: implications for assays of cardiolipin and mitochondrial mass. *J Neurochem*. 2002;82:224–233.
65. Keij JF, Bell-Prince C, Steinkamp JA. Staining of mitochondrial membranes with 10-nonyl acridine orange, MitoFluor Green, and MitoTracker Green is affected by mitochondrial membrane potential altering drugs. *Cytometry*. 2000;39:203–210.
66. Garcia Fernandez MI, Ceccarelli D, Muscatello U. Use of the fluorescent dye 10-N-nonyl acridine orange in quantitative and location assays of cardiolipin: a study on different experimental models. *Anal Biochem*. 2004;328:174–180.
67. Hennig S, Manstein DJ. Improvement of image resolution by combining enhanced confocal microscopy and quantum dot triexciton imaging. *FEBS Open Bio*. 2021;11:3324–3330.
68. mitoAnnotation C H Lee. https://github.com/shiown026/mitoAnnotation.

Supplementary Information

Mitochondria morphology analysis workflow

Supplement 1 demonstrates the workflow for mitochondrial morphology analysis used in this manuscript. The raw images were deconvoluted using the Airyscan super-resolution processing function with optimal auto-filter setting. Following deconvolution, a Gaussian blur filter was used to denoise the image, and a top hat morphological transformation was performed to subtract non-mitochondria objects using ImageJ. Recognition of mitochondria was determined by thresholding the image based on the intensity profile of each image. An unsupervised K-means algorithm was used to determine the intensity threshold value to accurately distinguish true mitochondria pixels from background fluorescence. The threshold segmentation process is mainly extracting foreground based on gray value information, which is especially useful for the segmentation of images with a strong contrast between foreground objects (mitochondria) and background. In the time-lapse experiments, the photobleaching effect will result in worse recognition of mitochondria due to the dim fluorescence. Therefore, the mitochondria objects were manually inspected and compared to the original images before further morphology analysis using ImageJ.

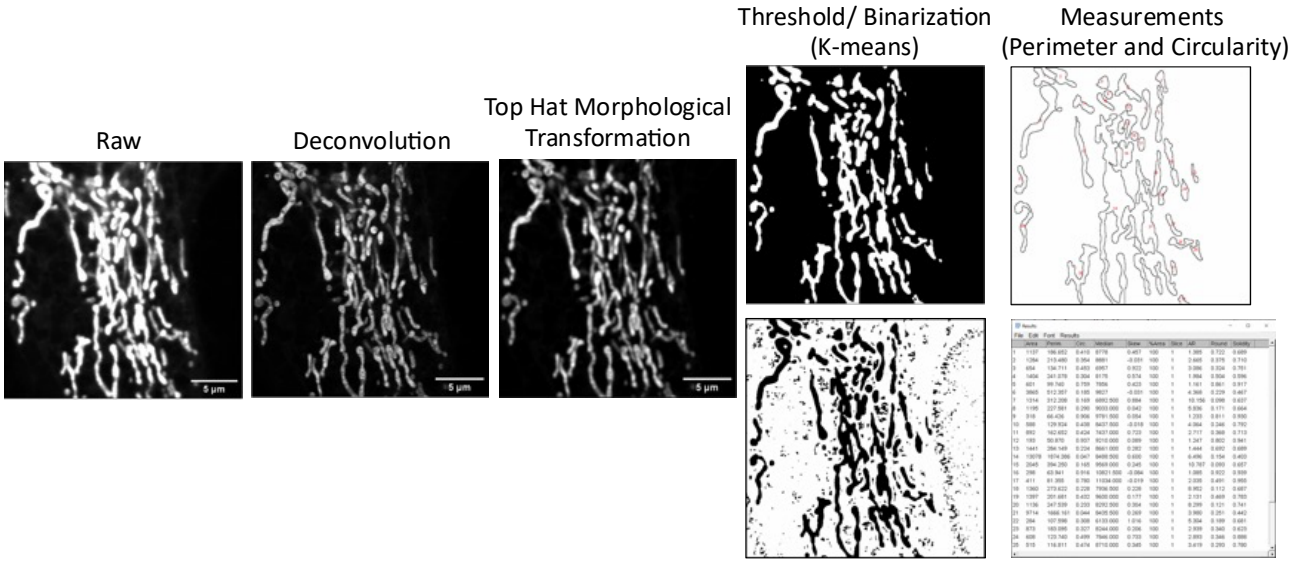

Supplement 1. Quantification design for tracking mitochondrial morphology using NAO. *The raw image was deconvoluted to get ultrafine structure information of mitochondria cristae. The top-hat morphological transformation subtracted out small, noisy, non-mitochondria objects. The unsupervised K-Means clustering algorithm separated the fluorescence intensity into two groups: mitochondria and non-mitochondria. The calculation of mitochondria perimeter and circularity was done by particle analysis application built-in ImageJ.*

488/ 561nm laser excitation to NAO and MTG dyes comparison

Here we compare the differences of cells stained with 1. NAO and TMRE or 2. MTG and TMRE exposed to 488 nm and 561 nm lasers under the same illumination conditions.

Supplement 2 shows the image results of mitochondria in HeLa, HEK293, and L6 cells stained with NAO and TMRE or MTG and TMRE, and excited by 488 nm and 561 nm laser under identical illumination and filter settings (0.5 % laser intensity and 3.54 μs dwell time per pixel) in time-lapse experiments. Cells stained with MTG showed a relatively higher resistance to photobleaching compared to those stained with NAO. Supplement 3 shows the comparison of HeLa cells stained with TMRE and NAO or MTG excited by 488 nm and 561 nm laser under identical illumination and filter settings (0.5 % laser intensity and 3.54 μs dwell time per pixel) in time-lapse experiments. For HeLa cells stained with NAO and TMRE, both NAO and TMRE fluorescence disappeared (decreased by over 90 %) after 10 images were taken. On the other hand, HeLa cells stained with TMRE and MTG remained over 50 % intensities of both fluorescences after 30 images were taken. The calculation of fluorescence intensity in each HeLa cells group using the whole image is shown in Supplement 2. An auto-threshold procedure (Otsu method) is first applied to segment out mitochondria from the background. Later, we averaged the whole values of the mitochondria pixels to get the averaged fluorescence intensity at each time point.

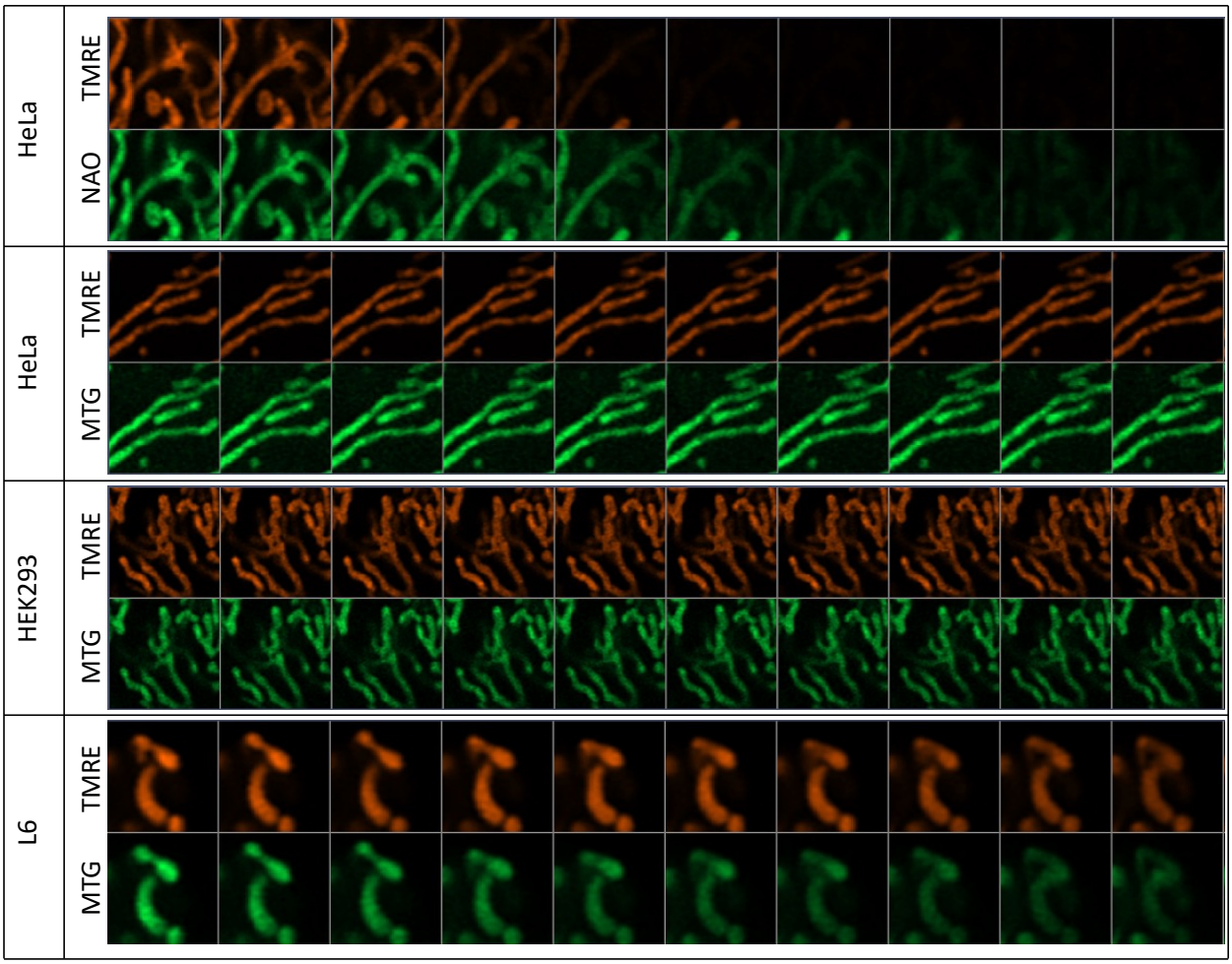

Supplement 2. Time-lapse images of mitochondria in HeLa, HEK293, and L6 cells stained with NAO and TMRE or MTG and TMRE, and excited by 488 nm and 561 nm laser in time-lapse experiments (Identical illumination and filter settings).

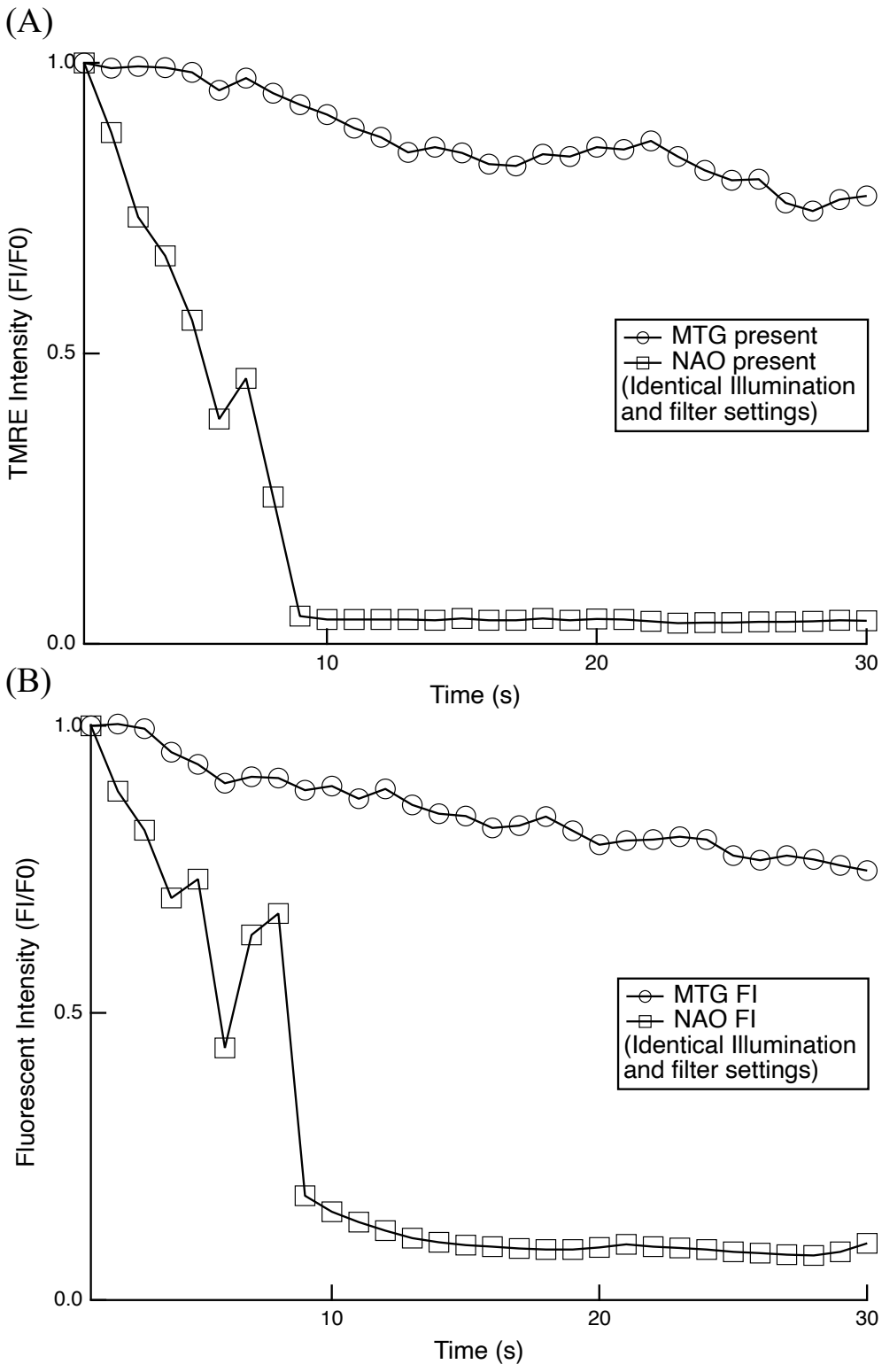

Supplement 3. Results of HeLa cells stained with TMRE and NAO or MTG, and excited by 488nm and 561nm laser for time-lapse imaging (Identical illumination and filter settings). (A) The percentage drop of TMRE fluorescence intensity versus time when NAO or MTG is present. (B) The percentage drop of MTG or NAO fluorescence intensity versus time.

Statistic table for experiments

For all figures in the main text, we present the following tables of how many times that experiment was performed, and under what conditions. This demonstrates in detail the reproducibility of all the key findings of this paper. In particular, this clearly establishes that we are indeed seeing a common phenomenon, and not just an exception.

Conclusion for Fig 1: "NAO performed a rapid loss of fluorescence compared to MTG"

Conclusion for Fig 2 and Fig 3: "NAO phototoxicity causes mitochondria ultrastructure to be destroyed and morphological changes from tubular shape to spherical shape."

Conclusion for Fig 4: "NAO phototoxicity is due to the exposure to 488 nm illumination, verified by loss of mitochondrial membrane potential."

Conclusion for Fig. 5 and Fig 6: "Long-term incubation of NAO dye does not cause potential cytotoxicity and the phototoxic effect is restricted to the illuminated region of the cells."

In Supplement Table 1, we list all time-lapse experiments of cells stained with NAO and TMRE dyes and exposed to 488 nm and/or 561 nm illuminations. In a total of 15 experiments, 10 of the 15 times (66.7%) we observed mitochondria swell after exposed to the illuminations. 14 of the 15 times (93%, the only one time was imaged without TMRE channel, no data for membrane potential) we observed a rapid loss of membrane potential after exposed to the illuminations. The rows in grey are cells exposed to 561 nm illumination only. 4 of the 4 times (100%) the mitochondria demonstrate neither morphological changes nor loss of mitochondrial membrane potential, which verified the NAO phototoxicity is due to the exposure to 488 nm illumination.

In Supplement Table 2, we list all time-lapse experiments of cells stained with MTG and TMRE dyes and exposed to 488 nm and/or 561 nm illuminations. In total 5 experiments, 5 of the 5 times (100%) we did not observe mitochondria swell after being exposed to the illuminations. The rapid loss of membrane potential was also not observed after exposed to the illuminations.

In Supplement Table 3, we list all experiments with long-term staining of cells with NAO and TMRE dyes. In total 3 experiments, 3 of the 3 times we observed neither the swelling of mitochondria nor the loss of membrane potential after 24 hours of incubation.

Record for time-lapse imaging with NAO+TMREdye											
Date	Cell used (Passage #)	Lables	Staining condition	Laser settings	Objective	Detection [nm]	Pixel time [us]	Pixel size [nm]	FOV [um]	Mitochondria swelling?	Rapid lost of membrane potential?
100121(001~003)	HeLa (P9)	TMRE NAO	10 nM; 15 min; DMEM 100 nM; 15 min; DMEM	λex561nm (0.3%) λex488nm (0.3%)	63x	561-700 488-560	5.31	42	398x398	Y	Y
100521(003,009)	HeLa (P10)	TMRE NAO	10 nM; 15 min; DMEM 100 nM; 15 min; DMEM	λex561nm (0.1%) λex488nm (0.1%)	63x	561-700 488-560	10.94	43	362x362	Y	Y
100921(009~011)	HeLa (P10)	TMRE NAO	10 nM; 15 min; DMEM 100 nM; 15 min; DMEM	λex561nm (0.2%) λex488nm (0.1%)	63x	561-700 488-560	3.55	43	12.68x12.68	Y	Y
101121(007~009)	HeLa (P11)	TMRE NAO	10 nM; 15 min; DMEM 100 nM; 15 min; DMEM	λex561nm (0.2%) λex488nm (0.2%)	63x	561-700 488-560	1.33	42	16.90x16.90	Y	Y
101321(004)	HeLa (P11)	TMRE NAO	10 nM; 15 min; DMEM 100 nM; 15 min; DMEM	λex561nm (0.3%) λex488nm (1.0%)	63x	561-700 488-560	17.79	43	10.14x10.14	Y	Y
101721(038)	HeLa (P13)	TMRE NAO	10 nM; 15 min; DMEM 100 nM; 15 min; DMEM	λex561nm (0.1%) λex488nm (0.05%)	63x	561-700 488-560	4.45	43	10.14x10.14	Y	Y
120821(012~014)	HeLa (P11)	TMRE NAO	10 nM; 15 min; DMEM 100 nM; 15 min; DMEM	λex561nm (0.3%)	63x	561-700	3.76	49	8.97x8.97	N	N
120921(003 004)	HeLa (P12)	TMRE NAO	10 nM; 15 min; DMEM 100 nM; 15 min; DMEM	λex561nm (0.5%)	63x	561-700	2.04	49	25.35x25.35	N	N
122121	HeLa (P14)	TMRE NAO	10 nM; 15 min; DMEM 100 nM; 15 min; DMEM	λex561nm (0.3%)	63x	561-700	3.76	49	8.97x8.97	N	N
021222(013~015)	HeLa (P5)	TMRE NAO	10 nM; 15 min; DMEM 100 nM; 15 min; DMEM	λex561nm (0.5%) λex488nm (0.3%)	63x	561-700 488-560	0.85	43	16.90x16.90	N	Y
050422(004)	HeLa (P10)	TMRE NAO	10 nM; 15 min; DMEM 100 nM; 15 min; DMEM	λex561nm (0.5%) λex488nm (0.5%)	63x	561-700 488-560	1.43	42	4.06x4.06	N	Y
050422(006)	HeLa (P10)	TMRE NAO	10 nM; 15 min; DMEM 100 nM; 15 min; DMEM	λex561nm (0.5%)	63x	561-700	1.65	49	3.9x3.9	N	N
050422(206)	L6 (P8)	TMRE NAO	10 nM; 15 min; DMEM 100 nM; 15 min; DMEM	λex561nm (0.5%) λex488nm (2.0%)	63x	561-700 488-560	1.79	42	4.06x4.06	N	Y
050422(211)	L6 (P8)	TMRE NAO	10 nM; 15 min; DMEM 100 nM; 15 min; DMEM	λex561nm (0.5%) λex488nm (2.0%)	63x	561-700 488-560	1.79	42	4.06x4.06	Y	Y
030823(104~106)	HeLa (P8)	TMRE NAO	10 nM; 15 min; DMEM 100 nM; 15 min; DMEM	λex561nm (1.0%) λex488nm (1.0%)	63x	561-700 488-560	1.15	43	77.01x78.01	N	Y
031723(108~110)	HeLa (P8)	TMRE NAO	10 nM; 15 min; DMEM 100 nM; 15 min; DMEM	λex561nm (1.0%) λex488nm (1.0%)	63x	561-700 488-560	0.98	43	15.88x15.88	N	Y
040523(108~110)	HeLa (P8)	TMRE NAO	10 nM; 15 min; DMEM 100 nM; 15 min; DMEM	λex561nm (1.0%) λex488nm (1.0%)	63x	561-700 488-560	0.98	43	15.88x15.88	N	Y
041123(310~312)	HEK293 (P10)	TMRE NAO	10 nM; 15 min; DMEM 100 nM; 15 min; DMEM	λex561nm (0.3%) λex488nm (0.3%)	63x	561-700 488-560	0.88	43	21.09x21.09	Y	Y

Supplement Table 1. Record and statistic table for experiments having cells stained with NAO and TMRE, and exposed to 488 nm and/or 561 nm illuminations.

Record for time-lapse imaging with MTG+TMRE dye excited by 488 nm and 561 nm illuminations											
Date	Cell used (Passage #)	Lables	Staining condition	Laser settings	Objective	Detection [nm]	Pixel time [us]	Pixel size [nm]	FOV [um]	Mitochondria swelling?	Rapid lost of membrane potential?
121021001	HeLa (P11)	TMRE MTG	10 nM; 15 min; DMEM 100 nM; 15 min; DMEM	λex561nm (0.5%) λex488nm (0.5%)	63x	561-700 488-560	3.54	43	25.35x25.35	N	N
121021004	HeLa (P11)	TMRE MTG	10 nM; 15 min; DMEM 100 nM; 15 min; DMEM	λex561nm (0.5%) λex488nm (1.0%)	63x	561-700 488-560	3.54	43	25.35x25.35	N	N
121321009	HeLa (P12)	TMRE MTG	10 nM; 15 min; DMEM 100 nM; 15 min; DMEM	λex561nm (0.1%) λex488nm (0.1%)	63x	561-700 488-560	3.55	43	11.66x11.66	N	N
121721018	HeLa (P8)	TMRE MTG	10 nM; 15 min; DMEM 100 nM; 15 min; DMEM	λex561nm (0.5%) λex488nm (0.1%)	63x	561-700 488-560	3.55	43	11.66x11.66	N	N
051022(009)	HeLa (P11)	TMRE MTG	10 nM; 15 min; DMEM 100 nM; 15 min; DMEM	λex561nm (1.0%) λex488nm (1.0%)	63x	561-700 488-560	2.63	41	4.34x4.34	N	N

Supplement Table 2. Record and statistic table for experiments having cells stained with MTG and TMRE, and exposed to 488 nm and/or 561 nm illuminations.

Record for 24-hours incubation with NAO+TMRE dye											
Date	Cell used (Passage #)	Lables	Staining condition	Laser settings	Objective	Detection [nm]	Pixel time [us]	Pixel size [nm]	FOV [um]	Mitochondria swelling?	Rapid lost of membrane potential?
042523(004)	HEK293 (P13)	TMRE NAO	10 nM; 15 min; DMEM 100 nM; 15 min; DMEM	λex561nm (1.0%) λex488nm (1.0%)	63x	561-700 488-560	1.15	74	245.73x245.73	N	N
042523(013)	HEK293 (P13)	TMRE NAO	10 nM; 15 min; DMEM 100 nM; 15 min; DMEM	λex561nm (1.0%) λex488nm (1.0%)	63x	561-700 488-560	1.15	43	78.01x78.01	N	N
042523(040)	HEK293 (P13)	TMRE NAO	10 nM; 15 min; DMEM 100 nM; 15 min; DMEM	λex561nm (1.0%) λex488nm (1.0%)	63x	561-700 488-560	0.93	43	48.19x48.19	N	N

Supplement Table 3. Record and statistic table for experiments of cells having long-term staining with NAO and TMRE.

Literature review: Prior Art

Mitochondria have commonly been employed as focal points for assessing microscopy techniques, as they offer opportunities to examine various aspects of an imaging system due to their intricate structure, structural diversity, and dynamic behavior. Furthermore, their susceptibility to photo stress makes them ideal subjects for evaluating the potential phototoxic effects of a specific approach. Supplement Table 4 and Supplement Table 5 include most but not all of the literature finding photobleaching and phototoxicity using super-resolution microscopy.

Minamikawa et al. [1] report that chloromethyl-X-rosamine (MitoTracker Red) exhibits significant photosensitizing properties. The exposure of intact cells containing chloromethyl-X-rosamine to light leads to the depolarization of the inner mitochondrial membrane and mitochondrial swelling, ultimately resulting in apoptosis. However, in colony formation tests, chloromethyl-X-rosamine itself demonstrated no toxicity within the concentration range of 100-250 nM, unless subjected to photoirradiation. The phototoxicity of chloromethyl-X-rosamine was found to be potent, as nearly complete cell death was achieved with light doses exceeding 2 J/cm^2. These light-damaged cells initially exhibited swollen and degenerative mitochondria, followed by the uptake of propidium iodide in their apoptotic nuclei.

Jaroslav et al. explained how phototoxicity influences live samples and highlighted that, besides the obvious effects of phototoxicity, there were often subtler consequences of illumination that were imperceptible when only the morphology of samples was examined.

Jaroslav presented strategies to reduce phototoxicity, including limiting the illumination to the focal plane and using pulsed illumination with longer wavelengths.

Wolf et al. [2] present a model in which cristae within the same mitochondrion behave as independent bioenergetic units. The different cristae within the individual mitochondrion can have disparate membrane potential. They present laser-induced depolarization time series from L6 myoblast stained with Rho123 (voltage-dependent dye) exposed to the phototoxic pulse of a 2-photon laser. The interventions causing acute depolarization may affect some cristae while sparing others

Wang et al. [3] developed a photostable fluorescent marker for STED microscopy, MitoPB Yellow, which had a high resistance to photobleaching and could remain in the membrane even after the loss of membrane potential. MitoPB Yellow allowed them to observe the mitochondrial ultrastructural change of the inner membrane in live cells undergoing apoptosis. Their observations revealed that, over an extended period of time, the mitochondria experienced swelling and the loss of cristae, which they attributed to photodamage induced by the intense STED laser.

Jakobs et al. provide an overview of recent studies using super-resolution microscopy to investigate mitochondria and discuss the strengths and opportunities of the various methods in addressing specific questions in mitochondrial biology.

Yang et al. [4] reported that mitochondria were susceptible to phototoxicity in long-term super-resolution imaging. They utilized Hessian-SIM microscopy to show that extensive illumination could induce rapid swelling of mitochondria, followed by the deformation and

abruption of inner-membrane cristae. Ultimately, mitochondria transformed into round, hollow structures.

Song et al. reported a synthetic approach to build novel methoxy modified Si-rhodamine (SiRMO) dyes as a photostable and bright organic dye emitting in the near-infrared region for long-term dynamic bioimaging. They observed the structure of mitochondrial cristae and mitochondria fission, fusion, and apoptosis with a high temporal resolution. Under two-photon illumination, SiRMO-2 showed also enhanced two-photon brightness and stability.

Yang et al. developed an enhanced squaraine variant dye (MitoESq-635) to study the dynamic structures of mitochondrial cristae in live cells with a superresolution technique. The low saturation intensity and high photostability of MitoESq-635 make it ideal for long-term, high-resolution (stimulated emission depletion) STED nanoscopy. They performed time-lapse imaging of the mitochondrial inner membrane over 50 min (3.9 s per frame, with 71.5 s dark recovery) in living HeLa cells with a resolution of 35.2 nm. The forms of the cristae during mitochondrial fusion and fission can be clearly observed.

Liu et al. [5] developed a photostable fluorescent dye, PKMO, which drastically reduced the photobleaching and phototoxicity effects compared to other fluorescent dyes. In their data on phototoxicity, the mitochondria demonstrated visible swelling and experienced a drop in mitochondrial membrane potential.

Year	Author	Title	Category	Microscopy	Sphericity
1999	Minamikawa.	Chloromethyl-X-rosamine (MitoTracker Red) photosensitises mitochondria and induces apoptosis in intact human cells.	Phototoxic	Confocal	X
2017	Jaroslav.	Phototoxicity in live fluorescence microscopy, and how to avoid it.	Photobleach	Confocal, light-sheet	
2019	Wolf.	Individual cristae within the same mitochondrion display different membrane potentials and are functionally independent.	Phototoxic	Airyscan	
2019	Wang.	A photostable fluorescent marker for the superresolution live imaging of the dynamic structure of the mitochondrial cristae.	Phototoxic	STED	X
2020	Jakobs.	Light Microscopy of Mitochondria at the Nanoscale.	Photobleach	STED	
2020	Yang.	Cyclooctatetraene-conjugated cyanine mitochondrial probes minimize phototoxicity in fluorescence and nanoscopic imaging.	Phototoxic	Hessian-SIM	X
2020	Song.	Improving Brightness and Stability of Si-Rhodamine for Super-Resolution Imaging of Mitochondria in Living Cells.	Photobleach	Airyscan, STED	
2020	Yang.	Mitochondrial dynamics quantitatively revealed by STED nanoscopy with an enhanced squaraine variant probe	Photobleach Phototoxic	STED	
2022	Liu.	Multi-color live-cell STED nanoscopy of mitochondria with a gentle inner membrane stain.	Phototoxic	STED	X

Supplement Table 4. Literature finding photobleaching and phototoxicity using super-resolution microscopy.

	Dye	Microscope	Image Resolution	Reference
Research	MitoPB Yellow	STED	45 nm	A photostable fluorescent marker for the superresolution live imaging of the dynamic structure of the mitochondrial cristae
	MitoESq-635	STED	35.2 nm	Mitochondrial dynamics quantitatively revealed by STED nanoscopy with an enhanced squaraine variant probe
	PKMO	STED	50 nm	Multi-color live-cell STED nanoscopy of mitochondria with a gentle inner membrane stain
	SiRMO-2	STED	N/A	Improving Brightness and Stability of Si-Rhodamine for Super-Resolution Imaging of Mitochondria in Living Cells
Commercial	MitoTracker DeepRed	Confocal/STED	50 nm (by experience)	https://www.thermofisher.com/order/catalog/product/M22426
	VSD-001	N/A	N/A	https://akitainnovations.com/products-services/voltage-sensitive-dyes/
	MitoBrilliant™ Live 646	Confocal/STED	N/A	https://www.tocris.com/products/mitobrilliant-live-646_7417
	TMRE	Confocal/STED	N/A	https://www.thermofisher.com/order/catalog/product/T669
	ABBERIOR LIVE ORANGE	STED	N/A	https://abberior.shop/abberior-LIVE-ORANGE

Supplement Table 5. Recent research and commercial structure dyes for super-resolution microscopy.

Excitation and Emission of NAO and MTG

Supplement 4 and Supplement 5 show the excitation and emission of the 10-N-nonyl acridine orange (NAO) dye and Mitotracker Green (MTG) dye.

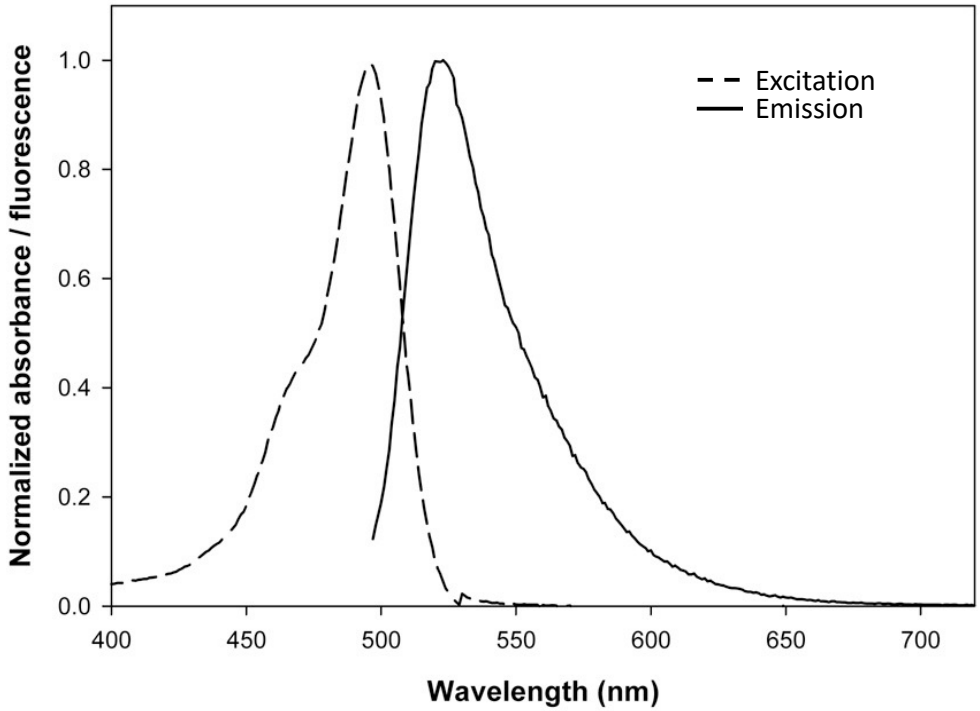

Supplement 4. Excitation and emission range for NAO dye. (https://europepmc.org/article/pmc/2585370)

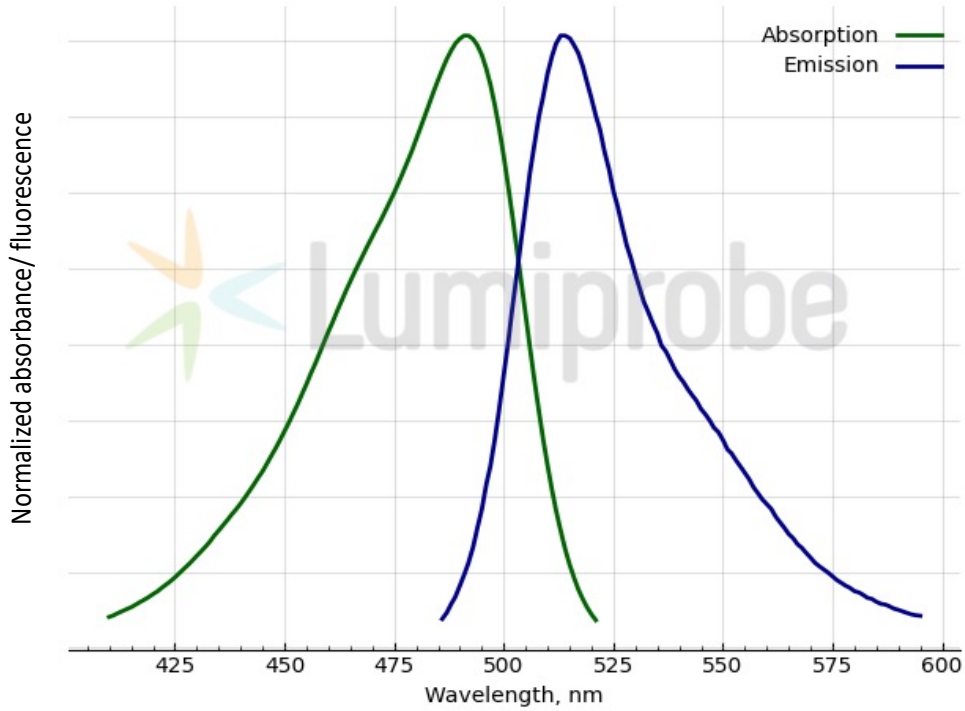

Supplement 5. Excitation and emission range for MTG dye. (https://www.lumiprobe.com/p/mitotracker-green-fm)

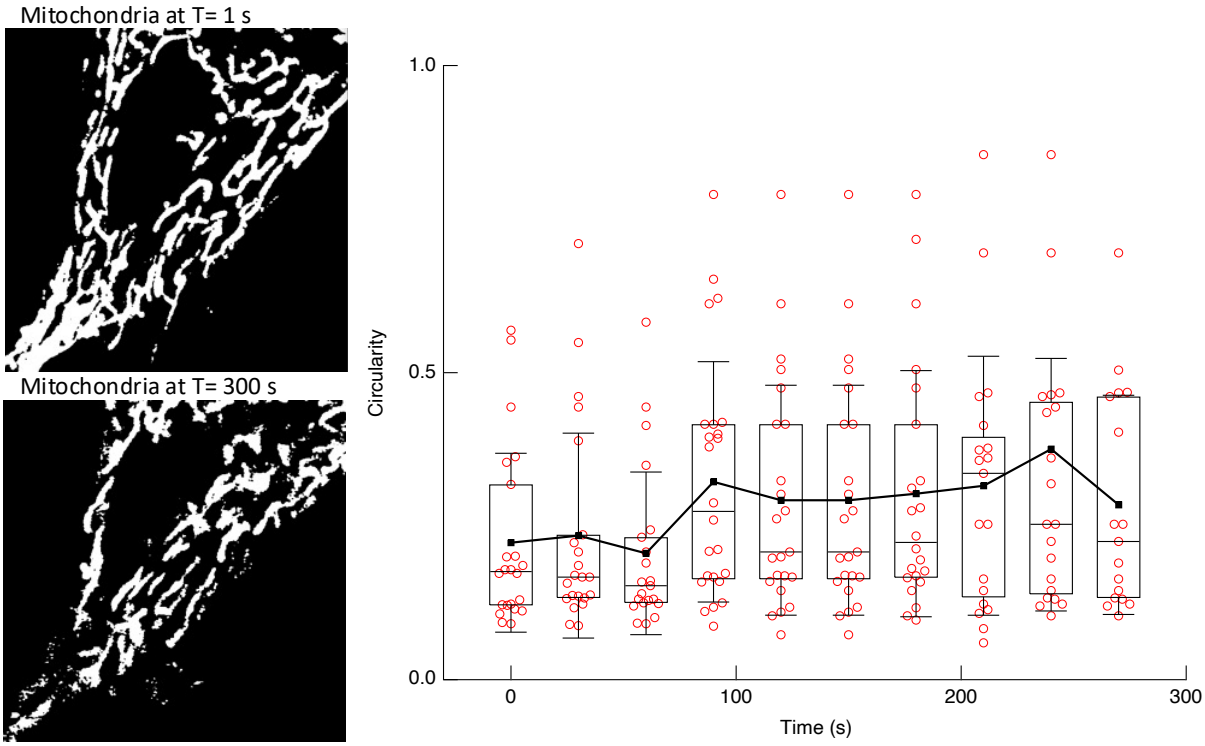

Supplement 6. Mitochondria segmentation and structure analysis. The binarization mask is used for single mitochondria analysis. The statistical analysis shows the change of circularity of mitochondria in cells through the time-lapse experiment. The mitochondria in the HeLa cell were stained with 100 nM MTG (Intensity: 0.5 %; Pixel time: 3.54 µs; Time frame: 1 s).

References

1. Minamikawa, T. *et al.* Chloromethyl-X-rosamine (MitoTracker Red) photosensitises mitochondria and induces apoptosis in intact human cells. *J Cell Sci* **112**, 2419–2430 (1999).
2. Wolf, D. M. *et al.* Individual cristae within the same mitochondrion display different membrane potentials and are functionally independent. *EMBO J* **38**, e101056 (2019).
3. Wang, C. *et al.* A photostable fluorescent marker for the superresolution live imaging of the dynamic structure of the mitochondrial cristae. *Proceedings of the National Academy of Sciences* **116**, 15817–15822 (2019).
4. Yang, Z. *et al.* Cyclooctatetraene-conjugated cyanine mitochondrial probes minimize phototoxicity in fluorescence and nanoscopic imaging. *Chem Sci* **11**, 8506–8516 (2020).
5. Liu, T. *et al.* Multi-color live-cell STED nanoscopy of mitochondria with a gentle inner membrane stain. *Proc Natl Acad Sci U S A* **119**, (2022).